PPPL-2252

UC20-G

PPPL-2252

ION TRANSPORT IN STELLARATORS

By

D.D.-M. Ho and R.M. Kulsrud

SEPTEMBER 1985

PLASMA PHYSICS LABORATORY

PRINCETON UNIVERSITY

PRINCETON, NEW JERSEY

PREPARED FOR THE U.S. DEPARTMENT OF ENERGY,
UNDER CONTRACT DE-AC02-76-CHO-3073.

ION TRANSPORT IN STELLARATORS

PPPL--2252

DE86 000575

D. D.-M. Hot and R. M. Kulsrud

Plasma Physics Laboratory, Princeton University

P.O. Box 451, Princeton, New Jersey 08544

Abstract

Stellarator ion transport in the low-collisionality regime with a radial electric field is calculated by a systematic expansion of the drift-Boltzmann equation. The shape of the helical well is taken into account in this calculation. It is found that the barely trapped ions with three to four times the thermal energy give the dominant contribution to the diffusion. Expressions for the ion particle and energy fluxes are derived.

† Present address: Lawrence Livermore National Laboratory, University of California, Livermore, CA 94550

I. Introduction

A kinetic calculation for stellarator ion transport in the low-collisionality regime is presented in this paper. This calculation is done using a systematic expansion of the drift-Boltzmann equation. The electron transport, the method for determining the self-consistent electric field, and the discussion of the overall stellarator transport problem are addressed in a companion paper.[1]

The shape of the helical magnetic well (from stellarator helical windings) is taken into account in the kinetic calculation. The behavior of ion transport at various pitch angles and energies, and the effect of collisionless detrapping/entrapping are discussed. The results show that the dominant contribution to ion transport comes from those barely trapped ions with three to four times the thermal energy. The stellarator ion transport was first studied by Galeev et al.[2] and by Galeev and Sagdeev.[3] Expanding their work, this paper presents results that were not discussed in their original studies. In addition, the ion diffusion coefficient given in this paper is smaller that that given in Ref. 3 by one order of magnitude. A factor of five of this discrepancy lies in the numerical integration over the proper energy weighting of the Maxwellian distribution function.

This paper is organized as follows. In Sec. II, the simplified magnetic field is given and the trajectories of trapped ions are discussed briefly. In Sec. III, the kinetic calculation of ion transport, with the shape of the helical wells approximated by rectangles, is presented. The expressions for ion particle and energy fluxes are derived in this section. An attempt to improve the numerical coefficient of the ion diffusion coefficient given in Sec. III is made in Sec. IV by using a more realistic magnetic well having a sinusoidal shape. Section V summarizes the results. In the Appendix, a

heuristic derivation of the ion diffusion coefficient with the effect of collisionless detrapping/entrapping is given.

II. Magnetic Field Geometry and Ion Orbits

As in Ref. 1, the magnetic surfaces are assumed to be nested circular tori. The simplified stellarator magnetic field strength has the form

$$B = B_0[1 - \varepsilon_h(r)\cos(\ell\theta - m\zeta) - \varepsilon_t \frac{r}{a}\cos\theta] \quad . \tag{1}$$

Here, ℓ is the multipolarity, m is the number of field periods, ε_t is the inverse aspect ratio (a/R_0), and ε_h is the depth of the helical windings. The toroidal coordinate system, in terms of minor radius r, poloidal angle θ, and the toroidal angle ζ, is shown in Fig. 1. Particles trapped in local helical wells have a grad-B drift component [caused by the toroidal field variation given by the third term in Eq. (1)] that is perpendicular to the magnetic surface, and this produces the major contribution to diffusion in a stellarator.

As shown in Ref. 1, an ambipolar radial electric field E_r arises from the fact that the ion's collisionality is much lower than the electron's. To estimate E_r, we use the approximation $E_r = -\partial\Phi/\partial r \approx [T/(en)](\partial n/\partial r)$. Using the stellarator parameters given in Table I, it can be shown that the poloidal $\vec{E}_r \times \vec{B}$ rotation frequency $Q_E \equiv c(E_r \times B)/rB^2$ is comparable to the effective collision frequency ν_{eff}. (This is the frequency for scattering across the trapping region in velocity space, and is equal to ε_h^{-1} times the ion collision frequency ν_i). Thus, the $\vec{E}_r \times \vec{B}$ drift can move most of the trapped ions, except those at very low energy, through several poloidal rotations during a collisional detrapping time.

Superposition of the grad-B drift upon the poloidal $\vec{E}_r \times \vec{B}$ drift results in an outward shift of the center of the trapped-ion drift orbit from the

center of the magnetic surface (see Fig. 2) by a distance

$$\Delta \equiv \frac{v_B}{\Omega_E} \quad ,$$

where v_B is the toroidal grad-B drift velocity.

In Ref. 1, it has been shown by a heuristic argument that the diffusion coefficient for ions without the effect of collisionless detrapping/entrapping (i.e., in the case where ε_h is constant throughout the minor radius) is

$$D_i \sim \frac{v_B^2}{\Omega_E} \left(\frac{\nu_i}{\Omega_E}\right)^{1/2} \quad . \tag{2}$$

Also, it is shown that the dominant contribution to ion diffusion comes from those barely trapped ions. This condition and the expression for D_i will be confirmed by a kinetic calculation in the following section.

In the following section, ε_h is treated as a constant. For most stellarators, however, the helical well depth ε_h increases with the minor radius r. Thus, ions may collisionlessly detrap out of and entrap into helical wells. As shown in the Appendix, for the reference stellarator, this effect is significant only for ions having energies more than roughly three times the thermal energy. In the later part of the following section, it is shown that the dominant contribution to ion diffusion, without the effect of collisionless detrapping/entrapping, comes from ions with energies between three and four times the thermal energy. Thus, for nonconstant ε_h, inclusion of the effect of collisionless detrapping/entrapping will give an estimate of the ion flux which is less than the estimate obtained without this effect. [The reason is that the ion diffusion coefficient is proportional to ν for the case with the effect of collisionless detrapping and entrapping but

proportional to $\nu^{1/2}$ for the case without this effect.] Nevertheless, the estimate obtained in the following section provides an upper bound for the ion flux.

III. Kinetic Calculation for Ion Transport with Rectangularly Shaped Magnetic Wells

The drift-Boltzmann equation is used to study the ion transport in the low-collisionality regime and is solved by a systematic expansion technique. If the magnetic field is time independent, then the drift-Boltzmann equation has the form

$$\frac{\partial f_i}{\partial t} + (\vec{v}_{\parallel} + \vec{v}_D)\cdot\vec{\nabla} f_i + e\frac{\partial \Phi}{\partial t}\frac{\partial f_i}{\partial \varepsilon} = C(f_i, f) \quad , \tag{3}$$

where the guiding center ion distribution function is

$$f_i = f_i(\varepsilon, u, \vec{r}, t) \ ,$$

the particle energy is

$$\varepsilon = \frac{m_i v^2}{2} + e\Phi \ ,$$

the magnetic moment is

$$\mu = \frac{m_i v_{\perp}^2}{2B} \ ,$$

the component of the particle drift velocity normal to a line of force is v_D,

and the position vector $\vec{r}$ is in (r,θ,ζ) coordinates. Each of the partial derivatives in Eq. (2) is to be taken by holding five of the six independent variables $\varepsilon,u,\vec{r},t$ constant.

Low collisionality means that trapped ions can bounce many times in a helical well before being detrapped by collisions. Thus, Eq. (3) can be solved by expanding f_i in terms of $1/v_\parallel$:

$$f_i = F_{i0} + F_{i1} + F_{i2} + \cdots \quad . \tag{4}$$

In Ref. 1, it has been shown that the solubility condition for the first-order uncrapped-particle distribution function $F_{i1}^{U.T.}$ is

$$\int_{shell} d\tau \frac{B}{v_\parallel} \left[\frac{\partial F_{i0}^{U.T.}}{\partial t} + e \frac{\partial \Phi}{\partial t} \frac{\partial F_{i0}^{U.T.}}{\partial \varepsilon} - C(F_{i0}^{U.T.}, F_0)\right] = 0 \ , \tag{5}$$

where the shell integral is over the volume between two neighboring magnetic surfaces. The solubility condition for the first-order trapped-particle distribution function $F_{i1}^{T.}$ is

$$\frac{\partial F_{i0}^{T.}}{\partial t} + \langle \vec{v}_D \rangle \cdot \vec{\nabla} F_{i0}^{T.} + e \frac{\partial \Phi}{\partial t} \frac{\partial F_{i0}^{T.}}{\partial \varepsilon} = \langle C(F_{i0}^{T.}, F_0) \rangle \ . \tag{6}$$

Here, the bounce-average operator

$$\langle \ldots \rangle \equiv \left(\oint d\ell / v\right)^{-1} \oint d\ell (\ldots)/v \quad ,$$

and

$$\langle \vec{v}_D \rangle = v_B(\sin\theta \, \hat{e}_r + \cos\theta \, \hat{e}_\theta) + r(\Omega_E + \Omega_H) \, \hat{e}_\theta \ ,$$

The poloidal drift due to helical ripples, Ω_H, is generally smaller than Ω_E, and thus can be ignored. (Note that for a rectangular-shaped helical well, the bounce average of a quantity is just equal to the quantity itself.)

As shown in Ref. 1, the boundary conditions for the distribution function just outside the thin boundary layer between the trapped and untrapped regions are:

$$f_i^{U.T.}(\xi_c^+) = f_i^{T.}(\xi_c^-) \tag{7a}$$

and

$$\int \frac{dS}{|\nabla p|} \frac{B}{v} \frac{\partial f_i}{\partial \xi}\bigg|_{\xi_c^+} = \int \frac{dS}{|\nabla p|} \frac{B}{v} \frac{\partial f_i}{\partial \xi}\bigg|_{\xi_c^-} \tag{7b}$$

where dS is a surface element on a magnetic surface and $\xi \equiv v_\parallel/v$ is the pitch-angle variable. The condition for trapping is $|\xi| < |\xi_c| \equiv (2\epsilon_h)^{1/2}$.

Equations (5) and (6) are still difficult to solve; therefore, it is necessary to further expand F_{i0}. Using the reference stellarator parameters, it can be shown that

$$\frac{v_B}{a\nu_{eff}} \sim \frac{v_B}{a\Omega_E} = \underline{O}(10^{-1}) \tag{8}$$

This ordering holds for ions with energies less than five times the thermal energy. Note that the ordering given by Eq. (8) is also valid in the recent experimental stellarators with parameters given in Table I. Thus, Eqs. (5) and (6) can be solved by expanding F_{i0} in powers of $v_B/a\nu_{eff}$ or $v_B/a\Omega_E$:

$$F_{i0} = f_{i0} + f_{i1} + f_{i2} + \cdots \tag{9}$$

Since the ion collision time is much less than the plasma confinement time, the ion distribution function is very close to a Maxwellian. This is formally shown by a Boltzmann H-theorem argument similar to that in Ref. 1. Thus,

$$f_{i0} = f_{iM}$$

$$= n_i \left(\frac{m_i}{2\pi T_i}\right)^{3/2} \exp\left(-\frac{\varepsilon - e\Phi}{T_i}\right) \quad , \tag{10}$$

where n_i, T_i, and Φ are functions of r and t.

For untrapped ions, the first-order equation is

$$\int_{\text{shell}} d\tau \frac{B}{v_\parallel} \sum_j C_{ij}(f_{i1}^{U,T.}) = 0 \quad . \tag{11}$$

For trapped ions, it is

$$< \sum_j C_{ij}(f_{i1}^{T.}) > = Q_E \frac{\partial f_{i1}^{T.}}{\partial \theta} + v_B \sin\theta \frac{\partial f_{iM}}{\partial r}\Big|_\varepsilon \quad . \tag{12}$$

In order to solve for $f_{i1}^{T.}$, let

$$f_{i1}^{T.} = \overline{f_{i1}^{T.}} + \mathcal{F}_i(\xi, \theta) \quad , \tag{13a}$$

with $\mathcal{F}_i(\xi_c, \theta) = 0$. As in Ref. 1, $f_{i1}^{U,T.}$ and $f_{i1}^{T.}$ can be taken to be zero. The function $\mathcal{F}_i$ can be assumed to have the form

$$\mathcal{F}_i = A(\xi)\sin\theta + B(\xi)\cos\theta \quad . \tag{13b}$$

The procedure for solving for $\mathcal{F}_i$ can be simplified by modeling the shape of the magnetic well as a rectangle with length and depth equal to the length and the maximum depth of the sinusoidal well. Using the results from this analysis, the behavior of $\mathcal{F}_i$ in a sinusoidal well can be studied in the asymptotic limit $\Omega_E/\nu_{eff} >> 1$ (see Sec. IV). The corresponding bounce-averaged pitch-angle scattering operator for the rectangularly shaped well is

$$< \sum_j C_{ij}(F_i) > = \frac{\sum_j \nu_{ij}}{4} \frac{\partial^2 \mathcal{F}_i}{\partial^2 \xi} \quad ,$$

where to a good approximation, the summation j is taken only over field ions. Using this simplified pitch-angle scattering operator, Eq. (12) becomes

$$\frac{\sum_j \nu_{ij}}{4} \frac{\partial^2 \mathcal{F}_i}{\partial \xi^2} = \Omega_E \frac{\partial \mathcal{F}_i}{\partial \theta} + v_B \sin\theta \left.\frac{\partial f_{iM}}{\partial r}\right|_\varepsilon \quad . \tag{14}$$

From Eq. (7b), the boundary conditions on $\mathcal{F}_i$ are

$$\oint d\theta \left.\frac{\partial \mathcal{F}_i}{\partial \xi}\right|_{\xi=\xi_c} = 0 \quad , \tag{15a}$$

and from before

$$\left.\mathcal{F}_i\right|_{\xi=\xi_c} = 0 \quad . \tag{15b}$$

Inserting Eq. (13b) into Eq. (14) and equating the $\sin\theta$ and $\cos\theta$ dependent terms, the resulting relations are:

$$\frac{\partial^2 A}{\partial \xi^2} + \frac{4}{\sum_j \nu_{ij}} \Omega_E B = \frac{4}{\sum_j \nu_{ij}} v_B \left.\frac{\partial f_{iM}}{\partial r}\right|_\varepsilon \quad ,$$

$$\frac{\partial^2 B}{\partial \xi^2} - \frac{4}{\sum_j \nu_{ij}} \Omega_E A = 0 \quad . \tag{16}$$

Taking even solutions to these two equations in ξ, we have:

$$\mathcal{F}_i = \left[a \cosh k\xi \cos k\xi - b \sinh k\xi \sin k\xi\right] \sin\theta$$

$$+ \left[a \sinh k\xi \sin k\xi + b \cosh k\xi \cos k\xi + \frac{\nu_B}{\Omega_E} \frac{\partial f_{iM}}{\partial r}\bigg|_\varepsilon\right] \cos\theta \quad . \tag{17}$$

In order to satisfy the boundary condition $\mathcal{F}_i\big|_{\xi=\xi_c} = 0$, each of the bracketed terms in front of the $\sin\theta$ and $\cos\theta$ terms in the above expression must vanish at $\xi = \xi_c$. Therefore,

$$a = -\frac{\nu_B}{\Omega_E} \frac{\sinh k\xi_c \sin k\xi_c}{\left(\sinh^2 k\xi_c \sin^2 k\xi_c + \cosh^2 k\xi_c \cos^2 k\xi_c\right)} \frac{\partial f_{iM}}{\partial r}\bigg|_\varepsilon$$

$$b = -\frac{\nu_B}{\Omega_E} \frac{\cosh k\xi_c \cos k\xi_c}{\left(\sinh^2 k\xi_c \sin^2 k\xi_c + \cosh^2 k\xi_c \cos^2 k\xi_c\right)} \frac{\partial f_{iM}}{\partial r}\bigg|_\varepsilon \quad . \tag{18}$$

To study the behavior of $\mathcal{F}_i$, the functions $A(\xi)\sin\theta$ and $B(\xi)\cos\theta$ are plotted [in units normalized by $(\nu_B/\Omega_E)(\partial f_{iM}/\partial r)$] versus the normalized pitch angle variable $\kappa \equiv \xi/\sqrt{2\varepsilon_h}$ at $\varepsilon = 4T$ in Fig. 3. The parameters are those of the reference stellarator, i.e., $\Omega_E/\nu_i \approx 45$ and $k \approx 10$ at $\varepsilon = 4T$. (The choice $\varepsilon = 4T$ is not arbitrary. As will be shown later, ions having approximately four times the thermal energy give the dominant contribution to ion energy diffusion.) Since terms involving $B(\xi)$ integrate to zero in the second order, we shall find that only the terms involving $A(\xi)$ contribute to diffusion. Figure 3 indicates that the function $A(\xi)$ peaks near $\kappa = 1$, $(\xi = \sqrt{2\varepsilon_h})$. This means that the dominant contribution to ion diffusion arises from the

barely trapped ions in helical wells as stated in Sec. II. Although the $B(\xi)$ term does not contribute directly to diffusion, this term creates a nonradial ambipolar electric field which causes enhancement of electron and ion diffusion (see Ref. 1).

The temporal evolution of the ion density and energy is obtained by going to second order in expansion (9). Integrate the second-order equations for trapped and untrapped ions with respect to ε and μ over the respective trapped and untrapped regions. Then, converting the line integral condition of the second-order trapped-ion equation into a shell integral condition, combining these two second-order equations, and using the conservation property of the collision operator gives

$$\int \frac{dS}{|\nabla P|} \int \frac{4\pi B d\mu d\varepsilon}{m_i^2 |v_\parallel|} \Big[\frac{\partial f_{iM}}{\partial t} + e\frac{\partial \Phi}{\partial \varepsilon}\frac{\partial f_{iM}}{\partial \varepsilon} + v_B \sin^2\theta \frac{\partial A}{\partial r} + v_B \cos^2\theta \frac{A}{r}$$

$$+ v_B \sin\theta \cos\theta \left(\frac{\partial B}{\partial r} - \frac{B}{r}\right) + \left(\Omega_E + \Omega_H\right) \frac{\partial f_{i1}^{T.}}{\partial \theta}\Big] = C \ , \tag{19}$$

Note that the $B(\xi)$ terms are odd in θ, and the Ω_E and Ω_H terms are complete integrals in θ. Hence, these terms vanish after surface integration. As in Ref. 1, Eq. (24) can be written in the particle conservation form, i.e.,

$$\frac{\partial \langle n_i \rangle}{\partial t} + \frac{1}{r}\frac{\partial}{\partial r} r\Gamma_i = 0 \ , \tag{20}$$

where the ion particle flux is

$$\Gamma_i = \frac{m\pi}{(2\pi)^2 R_0} \int_{-\pi/m}^{\pi/m} R_0 d\zeta \frac{4\sqrt{2}\pi}{m_i^{3/2}} \int_{e\Phi}^{\infty} d\varepsilon \sqrt{\varepsilon - e\Phi}\, v_B \int_0^{\xi_c} d\xi\, A(\xi,k) \ ,$$

$$= -\frac{1}{4\sqrt{2}} \frac{4\sqrt{2}\pi}{m_i^{3/2}} \int_{e\Phi}^{\infty} d\varepsilon \sqrt{\varepsilon - e\Phi}\, \frac{v_B^2}{\Omega_E} \left(\frac{\sum_j \nu_{ij}}{\Omega_E}\right)^{1/2} \mathcal{H} \left.\frac{\partial f_{iM}}{\partial r}\right|_\varepsilon \ , \tag{21}$$

where

$$\mathcal{K} \equiv \left(\frac{1}{\sinh^2 k\xi_c \sin^2 k\xi_c + \cosh^2 k\xi_c \cos^2 k\xi_c}\right)$$

$$\times \left[\sinh k\xi_c \sin k\xi_c \left(\sinh k\xi_c \cos k\xi_c + \cosh k\xi_c \sin k\xi_c\right)\right.$$

$$\left. - \cosh k\xi_c \cos k\xi_c \left(\cosh k\xi_c \sin k\xi_c - \sinh k\xi_c \cos k\xi_c\right)\right] \quad . \qquad (22)$$

Since $k >> 1$ at $\varepsilon \approx 4T$, Eq. (22) can be simplified by letting $k \to \infty$. Taking this limit gives:

$$\lim_{k\to\infty} \kappa = 1, \qquad \text{the "rotational limit."} \qquad (23a)$$

Taking the opposite limit, namely $k \to 0$ when $\varepsilon < T$, gives

$$\lim_{k\to 0} \kappa = \frac{2}{3} k^3 \xi_c^3 \ , \qquad \text{the "nonrotational limit."} \qquad (23b)$$

The integral in Eq. (21) can be estimated by making use of the rotational approximation (23a) above a "transition energy" ε_T and the nonrotational approximation (23b) below it. The "transition energy" ε_T is defined as the energy at which the ion particle flux from the rotational approximation equals that from the nonrotational approximation. [Note that ε_T is essentially the energy at which $\Omega_E = O(\nu_{eff})$]. Thus, Eq. (21) becomes

$$\Gamma_i = -\frac{1}{3}\left(2\varepsilon_h(r)\right)^{3/2} \frac{4\sqrt{2\pi}}{m_i^{3/2}} \int_{e\Phi}^{\varepsilon_T} d\varepsilon \sqrt{\varepsilon - e\Phi} \left.\frac{v_B^2}{\sum_j \nu_{ij}} \frac{\partial f_{iM}}{\partial r}\right|_\varepsilon$$

$$- \frac{1}{4\sqrt{2}} \frac{4\sqrt{2}\pi}{m_i^{3/2}} \int_{\varepsilon_T}^{\infty} d\varepsilon \sqrt{\varepsilon - e\Phi}\, \frac{v_B^2}{Q_E} \left(\frac{\sum_j \nu_{ij}}{Q_E} \right)^{1/2} \left. \frac{\partial f_{iM}}{\partial r} \right|_{\varepsilon} . \qquad (24)$$

The first term on the right-hand side of Eq. (24) has the same functional form as the electron particle flux given by Eq. (52) in Ref. 1 with a different numerical coefficient. This difference arises from the adoption of the rectangularly shaped magnetic well approximation. Since the actual result should agree with the result obtained using a sinusoidally shaped well, we simply replace the coefficient 1/3 by $4/9\pi$ from Eq. (52) in Ref. 1. From the second term on the right-hand side of Eq. (24), the ion diffusion coefficient at energies greater than ε_T is found to be proportional to $(v_B^2/Q_E)\,(\sum_j \nu_{ij}/Q_E)^{1/2}$. Thus, the detailed calculation confirms the result from the heuristic argument. An attempt to improve the numerical coefficient in front of the second term of Eq. (24) is made in Sec. IV by using a more realistic magnetic well having a sinusoidal shape. The result indicates that the correct coefficient should be $0.44/4\sqrt{2}$ instead of $1/4\sqrt{2}$. Thus, the ion particle flux per unit area with the proper numerical coefficient for a sinusoidally shaped magnetic well is

$$\Gamma_i = - \frac{4}{9\pi} \left(2\varepsilon_h(r)\right)^{3/2} \frac{4\sqrt{2}\pi}{m_i^{3/2}} \int_{e\Phi}^{\varepsilon_T} d\varepsilon \sqrt{\varepsilon - e\Phi}\, \frac{v_B^2}{\sum_j \nu_{ij}} \left. \frac{\partial f_{iM}}{\partial r} \right|_{\varepsilon}$$

$$- \frac{0.44}{4\sqrt{2}} \frac{4\sqrt{2}\pi}{m_i^{3/2}} \int_{\varepsilon_T}^{\infty} d\varepsilon \sqrt{\varepsilon - e\Phi}\, \frac{v_B^2}{Q_E} \left(\frac{\sum_j \nu_{ij}}{Q_E} \right)^{1/2} \left. \frac{\partial f_{iM}}{\partial r} \right|_{\varepsilon} . \qquad (25)$$

This equation can be applied to either deuteron or triton diffusion.

The integrals in Eq. (25) will now be evaluated. Note that in the asymptotic limit ($\sqrt{m_i/m_e} \gg 1$) the reciprocal of the 90° "deflection time" for deuterons scattered by field particles has the form

$$\sum_j \nu_{Dj}(v) = \nu_{DD}(v) + \nu_{DT}(v) \quad ,$$

$$= A_D \ell_D^3 \frac{\left[\left(\Phi(\sqrt{x}) - G(\sqrt{x})\right) + \left(\Phi(\sqrt{(m_T/m_D)x}) - G(\sqrt{(m_T/m_D)x})\right)\right]}{x^{3/2}} \quad , \tag{26}$$

Here,

$$A_D \equiv \frac{8\pi e^4 Z^2 Z_j^2 n_j \ln\Lambda}{m_i^2} \quad ,$$

$$\ell_D \equiv \left(\frac{m_D}{2T}\right)^{1/2} \quad ,$$

the Chandrasekhar function

$$G(\sqrt{x}) \equiv \frac{\Phi(\sqrt{x}) - \sqrt{x}\,\Phi'(\sqrt{x})}{2x} \quad ,$$

the usual error function

$$\Phi(\sqrt{x}) \equiv \frac{2}{\sqrt{\pi}} \int_0^{\sqrt{x}} e^{-y^2}\, dy \quad ,$$

$$x = \frac{\varepsilon - e\Phi}{T} \quad ,$$

and m_D is the deuterium mass.

Using Eq. (26), Eq. (25) can be written for deuterons as

$$\Gamma_D = -\frac{4}{9\pi}\left(\frac{cT}{eB_0R_0}\right)^2 \frac{\left(2\varepsilon_h(r)\right)^{3/2}}{A_D\ell_D^3} n_D \left\{\int_0^{x_T} dx\sqrt{x}\, \frac{x^{7/2}e^{-x}}{\sum_j \left(\Phi(\sqrt{x_j}) - G(\sqrt{x_j})\right)}\right.$$

$$\times \left[\frac{1}{n_D}\frac{\partial n_D}{\partial r} + \frac{e}{T}\frac{\partial \Phi}{\partial r} + (x - \frac{3}{2})\frac{1}{T}\frac{\partial T}{\partial r}\right]$$

$$+ \frac{0.44}{4\sqrt{2}}\left[\left(\frac{cT}{eB_0R_0}\right)^2/\Omega_E\right]\left(\frac{A_D\ell_D^3}{\Omega_E}\right)^{1/2} n_D \int_{x_T}^{\infty} dx\sqrt{x}\, x^{5/4}\, e^{-x}$$

$$\times \left[\sum_j\left(\Phi(\sqrt{x_j}) - G(\sqrt{x_j})\right)\right]^{1/2}\left[\frac{1}{n_D}\frac{\partial n_D}{\partial r} + \frac{e}{T}\frac{\partial \Phi}{\partial r} + (x - \frac{3}{2})\frac{1}{T}\frac{\partial T}{\partial r}\right]\Bigg\}$$

$$\div \int_0^{\infty} dx\sqrt{x}\, e^{-x} \quad . \tag{27}$$

To derive the equation for conservation of energy, the second-order equations for trapped ions and untrapped ions are multiplied by $m_i v^2/2$ and then a similar procedure to that employed in obtaining the particle conservation equation is used. The resulting energy conservation equation has the form

$$\frac{\partial}{\partial t}\frac{3}{2}\langle n_i T_i\rangle + \frac{1}{r}\frac{\partial}{\partial r} rQ_i + e\Gamma_i \frac{\partial \Phi}{\partial r} = 0 \quad . \tag{28}$$

The energy flux per unit area at a given minor radius for the deuteron is

$$Q_i = -\frac{4}{9\pi}\left(\frac{cT}{eB_0R_0}\right)^2 \frac{\left(2\varepsilon_h(r)\right)^{3/2}}{A_D\ell_D^3} n_D T \int_{x_T}^{\infty} dx\sqrt{x}\, \frac{x^{9/2}e^{-x}}{\sum_j\left(\Phi(\sqrt{x_j}) - G(\sqrt{x_j})\right)}$$

$$\times \left[\frac{1}{n_D}\frac{\partial n_D}{\partial r} + \frac{e}{T}\frac{\partial \Phi}{\partial r} + (x - \frac{3}{2})\frac{1}{T}\frac{\partial T}{\partial r}\right]$$

$$+ \frac{0.44}{4\sqrt{2}}\left[\left(\frac{cT}{eB_0R_0}\right)^2/\Omega_E\right]\left(\frac{A_D\ell_D^3}{\Omega_E}\right)^{1/2} n_D T \int_{x_T}^{\infty} dx\sqrt{x}\, x^{9/4} e^{-x}$$

$$\times \left[\sum_j\left(\Phi(\sqrt{x_j}) - G(\sqrt{x_j})\right)\right]^{1/2}\left[\frac{1}{n_D}\frac{\partial n_D}{\partial r} + \frac{e}{T}\frac{\partial \Phi}{\partial r} + (x - \frac{3}{2})\frac{1}{T}\frac{\partial T}{\partial R}\right]\Bigg\}$$

$$\div \int_0^{\infty} dx\sqrt{x}\, e^{-x} \quad . \tag{29}$$

Note that X_T is generally less than unity (see Ref. 1); thus, ion fluxes can be well approximated by keeping only the second term (the rotational limit) on the right-hand side of Eqs. (27) and (29). Comparing the value of the second term on the right-hand side of Eq. (27) to that of Eq. (21) at each energy shows that they are essentially equal unless $\varepsilon_T < T$. Therefore, the rotational limit is a very good approximation to the exact solution given by Eq. (21). To display the contribution to particle and energy diffusion that is due to deuterons with energy between ε and $\varepsilon+d\varepsilon$, the integrands in the second term on the right-hand side of Eqs. (27) and (29) are plotted versus energy. Assuming $(1/n)(\partial n/\partial r) = (e/T)(\partial\Phi/\partial r) = (1/T)(\partial T/\partial r)$, the integrands become $x^{7/4}e^{-x}[\Phi(\sqrt{x}) - G(\sqrt{x})]^{1/2}(x - 3/2)$ and $x^{11/4}e^{-x}[\Phi(\sqrt{x}) - G(\sqrt{x})]^{1/2}(x - 3/2)$, respectively. These are plotted versus x in Fig. 4. The figure shows that deuterons with roughly three and a half times the thermal energy give the dominant contribution to particle diffusion while those with roughly four times the thermal energy give the dominant contribution to energy diffusion. These figures also indicate that at low energies, the ion diffusion is inward. The reason is that ion mobility in E_r reduces the ion flux.

After numerically integrating the second terms of Eqs. (27) and (29) from zero to infinity, we find the approximate deuteron particle and energy fluxes (assuming a 50% - 50% D-T plasma) are:

$$\Gamma_D \simeq -\frac{0.44}{4\sqrt{2}}\left[\left(\frac{cT}{eB_0R_0}\right)^2/\Omega_E\right]\left(\frac{A_D\ell_D^3}{\Omega_E}\right)^{1/2} n_D\left[1.63\left(\frac{1}{n_D}\frac{\partial n_D}{\partial r} + \frac{e}{T}\frac{\partial\Phi}{\partial r} - \frac{3}{2}\frac{1}{T}\frac{\partial T}{\partial r}\right) + 4.63\,\frac{1}{T}\frac{\partial T}{\partial r}\right], \tag{30a}$$

$$Q_D \simeq -\frac{0.44}{4\sqrt{2}}\left[\left(\frac{cT}{eB_0R_0}\right)^2/\Omega_E\right]\left(\frac{A_D\ell_D^3}{\Omega_E}\right)^{1/2} n_D T\left[4.63\left(\frac{1}{n_D}\frac{\partial n_D}{\partial r}\right.\right.$$

$$+ \frac{e}{T}\frac{\partial\Phi}{\partial r} - \frac{3}{2}\frac{1}{T}\frac{\partial T}{\partial r}\Big) + 17.68\,\frac{1}{T}\frac{\partial T}{\partial r}\Big] \quad . \tag{30b}$$

It can be shown that the triton fluxes are nearly equal to the deuteron fluxes. Thus, deuteron fluxes can be used to estimate the ion particle and energy confinement times. However, for steady-state reactor operation, the deuterium and tritium injection ratio may be different from n_D/n_T and proper adjustment needs to be made. From Eq. (30), the ion diffusion coefficient is $0.13\{[cT/(eBR)]^2/Q_E\}(A_D\ell_D^3/Q_E)^{1/2}$ which is smaller than that given in Ref. 3 by an order of magnitude. A factor of five of this discrepancy lies in the numerical integration over the proper energy weighting of the Maxwellian distribution function.

Substitution of $A_D\ell_D^3$ into Eqs. (30a) and (30b) gives

$$\Gamma_D \cong -3.7\left(\frac{r_m}{\partial\Phi/\partial r_m}\right)^{3/2}\frac{n_{14}^{3/2}T_4^{7/4}}{B_4^{1/2}R_m^2}\Big[1.63\left(\frac{1}{n_{14}}\frac{\partial n_{14}}{\partial r_m}\right)$$

$$+ \frac{e}{T_4}\frac{\partial\Phi}{\partial r_m} - \frac{3}{2}\frac{1}{T_4}\frac{\partial T_4}{\partial r_m}\Big) + 4.63\,\frac{1}{T_4}\frac{\partial T_4}{\partial r_m}\Big]\ (10^{19}\ \mathrm{cm^{-2}\cdot sec^{-1}}) \ , \tag{31a}$$

$$Q_D \cong -3.7\left(\frac{r_m}{\partial\Phi/\partial r_m}\right)^{3/2}\frac{n_{14}^{3/2}T_4^{9/4}}{B_4^{1/2}R_m^2}\Big[4.63\left(\frac{1}{n_{14}}\frac{\partial n_{14}}{\partial r_m}\right.$$

$$\left. + \frac{e}{T_4}\frac{\partial\Phi}{\partial r}_m - \frac{3}{2}\frac{1}{T_4}\frac{\partial T_4}{\partial r_m}\right) + 17.68\,\frac{1}{T_4}\frac{\partial T_4}{\partial r_m}\Big]\ (10^{20}\ \mathrm{keV\cdot cm^{-3}\cdot sec^{-1}}) \ . \tag{31b}$$

Finally, Eqs. (31a) and (31b) can be cast to a matrix form that possesses Onsager symmetry in the electron case only.

IV. Ion Transport with a Sinusoidally Shaped Magnetic Well

The ion transport calculation presented in Sec. III has been simplified by modeling the shape of a magnetic well as a rectangle. In this section, an attempt is made to improve the previous calculation in the $\Omega_E/\nu_i \gg 1$ regime by using a more realistic magnetic well with sinusoidal shape. It has been shown in Sec. III that as $\Omega_E/\nu_i \gg 1$, the barely trapped ions give the dominant contribution to diffusion. Under this condition, the pitch-angle scattering operator can be simplified and the ion transport calculation with a sinusoidally shaped helical well can be carried out analytically.

For a sinusoidally shaped well, start with the first-order [in expansion (9)] bounce-averaged equation for the trapped ions [i.e., Eq. (12)]. The resulting equation is analogous to Eq. (19) and has the form

$$\frac{\Sigma_j \nu_{ij}}{4J} \frac{\partial}{\partial \xi_0} JD \frac{\partial \mathcal{F}_i}{\partial \xi_0} = \Omega_E \frac{\partial \mathcal{F}_i}{\partial \theta} + v_B \sin\theta \left. \frac{\partial f_{iM}}{\partial r} \right|_\varepsilon . \tag{32}$$

The functions ξ_0, D, and J are obtained by performing the bounce average for a sinusoidally shaped magnetic well, and have the following form (see Ref. 1):

$$\xi_0 \equiv \left(\frac{\varepsilon - \mu B + e\Phi}{\varepsilon}\right)^{1/2} \approx \frac{v_\parallel}{v} \quad \text{at the center of a magnetic well}$$

$$D \equiv (\kappa^2)^{-1} \left[\frac{E(\kappa)}{K(\kappa)} + (\kappa^2 - 1)\right] ,$$

$$\kappa \equiv \frac{\xi_0}{(2\varepsilon_h)^{1/2}} ,$$

and

$$J \equiv \frac{2\kappa K(\kappa) R}{m} .$$

The functions $K(\kappa)$ and $E(\kappa)$ are the complete elliptical integrals of the first and second kind, respectively.

Figure 3 indicates that in the rotational limit, the $\sin\theta$ part of the first-order distribution function peaks near $\kappa=1$. As κ approaches unity, the second term vanishes more rapidly than the first in the expression for D, therefore D can be approximated by

$$D \tilde{=} \frac{1}{K(\kappa_p)} \quad , \tag{33}$$

where κ_p is the location of the peak of the $\sin\theta$ part of the first-order distribution function. Also note that

$$\lim_{\kappa \to 1} \left\{ K(\kappa) - \frac{1}{2} \ln\left[16/(1-\kappa)\right] \right\} = 0 \quad . \tag{34}$$

Thus, near $\kappa = 1$, the derivative $[\partial(JD)/\partial\xi_0](\partial F_i/\partial\xi_0)$ is much smaller than $(JD)(\partial^2 F_i/\partial\xi_0^2)$ and Eq. (32) can be approximated by

$$\frac{\sum_j \nu_{ij}}{4K(\kappa_p)} \frac{\partial^2 \mathcal{F}_i}{\partial \xi_0^2} = \Omega_E \frac{\partial \mathcal{F}_i}{\partial \theta} + \nu_B \sin\theta \left. \frac{\partial f_{iM}}{\partial r} \right|_\varepsilon \quad . \tag{35}$$

[Although Eq. (34) has a logarithmic singularity at $\kappa = 1$, the value $1/K(\kappa_p)$ is finite since κ_p is not exactly equal to unity.]

In the rotational limit, the dominant contribution to diffusion is concentrated in a region of width $\underline{O}(\sqrt{\nu_i/\Omega_E})$ near $\kappa \sim 1$. Thus, the ξ_0 variable can be transformed into a "boundary-layer" variable x, which is defined as,

$$x = \frac{\xi_0 - \xi_c}{\epsilon_b} \quad , \; -\infty < x \leq 0 \tag{36a}$$

or

$$x\epsilon_b = (\kappa - 1)\xi_c \; , \tag{36b}$$

where

$$\epsilon_b \equiv \left(\frac{\sum_j \nu_{ij}}{4K(\kappa_p)\Omega_E}\right)^{1/2} << 1 \quad .$$

Expressing Eq. (35) in terms of the variable x gives

$$\frac{\partial^2 \mathfrak{F}_i}{\partial x^2} = \frac{\partial \mathfrak{F}_i}{\partial \theta} + \frac{v_B}{\Omega_E} \sin\theta \left.\frac{\partial f_{iM}}{\partial r}\right|_\varepsilon \quad . \tag{37}$$

Let

$$\mathfrak{F}_i = A(x)\sin\theta + B(x)\cos\theta \quad , \tag{38}$$

with boundary conditions on $\mathfrak{F}_i$ at $x = 0$ the same as the boundary conditions Eqs. (15a) and (15b). Then, using the same procedure employed in solving Eq. (16), it can be shown that in order to satisfy Eq. (37) and the boundary conditions, functions A(x) and B(x) must have the form:

$$A(x) = \frac{v_B}{\Omega_E} e^{x/\sqrt{2}} \sin\frac{x}{\sqrt{2}} \left.\frac{\partial f_{iM}}{\partial r}\right|_\varepsilon \quad , \tag{39a}$$

$$B(x) = \frac{v_B}{\Omega_E} \left(1 - e^{x/\sqrt{2}} \cos\frac{x}{\sqrt{2}} \left.\frac{\partial f_{iM}}{\partial r}\right|_\varepsilon\right) \quad . \tag{39b}$$

Thus, from Eq. (21), the ion particle flux per unit area is

$$\Gamma_i = \frac{m\pi}{(2\pi)^2 R_0} \int_{-\pi/m}^{\pi/m} R_0 d\zeta \, \frac{4\sqrt{2}\pi}{m_i^{3/2}} \int_0^{\infty} d\varepsilon \, \sqrt{\varepsilon - e\Phi} \, v_B \int_0^{\xi_c} d\xi \, A(x) \quad .$$

Note that $J = \int_{-\pi/m}^{\pi/m} (d\xi/d\xi_0) R_0 d\zeta = (2\kappa K(\kappa) R)/m$ as indicated in the Appendix of Ref. 1. Therefore, in the above equation

$$\int_{-\pi/m}^{\pi/m} R_0 d\zeta \int_0^{\xi_c} A(x) d\xi = \int_0^{\xi_c} JA(x) d\xi_0 \quad ,$$

$$= \epsilon_b \int_{\infty}^{0} JA(x) dx \quad .$$

Substituting Eq. (39b) into this expression gives

$$\epsilon_b \int_{-\infty}^{0} JA(x) dx \cong - \frac{1}{\sqrt{2}} \frac{R}{m} \kappa_p \sqrt{K(\kappa_p)} \, \frac{v_B^2}{\Omega_E} \left(\frac{\sum_j \nu_{ij}}{\Omega_E} \right)^{1/2} \left. \frac{\partial f_{iM}}{\partial r} \right|_{\varepsilon} \quad .$$

Thus, the ion particle flux is

$$\Gamma_i = - \frac{1}{4\sqrt{2}} \left(\frac{\kappa_p \sqrt{K(\kappa_p)}}{\pi} \right) \frac{4\sqrt{2}\,\pi}{m_i^{3/2}} \int_0^{\infty} d\varepsilon \sqrt{\varepsilon - e\Phi} \, \frac{v_B}{\Omega_E} \left(\frac{\sum_j \nu_{ij}}{\Omega_E} \right)^{1/2} \left. \frac{\partial f_{iM}}{\partial r} \right|_{\varepsilon} \quad . \qquad (40)$$

This equation differs from the second term on the right-hand side of Eq. (24) by the correction factor $\kappa_p \sqrt{K(\kappa_p)}/\pi$. The value of $\kappa_p K(\kappa_p)$ is evaluated by the following iterative procedure.

The value of κ to be used in the first step of the iteration is 0.8, which is the location of the peak of the $A(x)\sin\theta$ curve as shown in Fig. 3a. Then, from Eq. (34), $K(0.8) \approx 2.2$. The second step in the iteration is to use this value of K and Eq. (36b) to obtain a new value of κ. Note that the value of A in Eq. (39a) peaks at $x = -\sqrt{2}\pi/4$. If $x = -\sqrt{2}\pi/4$, $\epsilon_b \approx 0.05$ (taken at

$\varepsilon=4T$, the location of the peak of the curve as shown in Fig. 4), and $\xi_c=\sqrt{0.2}$, then Eq. (36b) gives $\kappa = 0.87$. This scheme converges rapidly. After two more iterations, K converges to a value of 2.5 as κ_p approaches 0.88. The correction factor at $\kappa_p = 0.88$ is then

$$\frac{\kappa_p\sqrt{K(\kappa_p)}}{\pi} = 0.44 \quad . \tag{41}$$

As expected, this correction factor is less than unity since fewer particles can be trapped in a sinusoidally shaped well than in a rectangularly shaped well with length and depth equal to the length and the maximum depth of the sinusoidal well.

V. Summary

For the various size stellarators studied, it is found that the $\vec{E}_r \times \vec{B}$ drift can always move most of the trapped ions through several poloidal rotations within a collisional detrapping time. The radial electric field is very effective in reducing ion fluxes because the diffusion coefficient is proportional to $\Omega_E^{-1.5}$. The dominant contribution to diffusion is from the barely trapped ions with three to four times the thermal energy. For a reactor plasma, the effect of collisionless detrapping/entrapping is important only when the ion energy becomes greater than approximately three times the thermal energy. The ion diffusion coefficient obtained in this paper is smaller than that given in Ref. 3 by one order of magnitude after the numerical integration for the energy weighting of the Maxwellian distribution function is carried out correctly. The results of this paper are applied in Ref. 1 to determine the self-consistent radial ambipolar electric field. It is shown there that the ion energy loss is comparable to that of the electrons.

Acknowledgements: This work was supported by United States Contract No. DE-AC02-76-CHO-3073.

Appendix : HEURISTIC DERIVATION OF THE ION DIFFUSION COEFFICIENT WITH THE EFFECT OF COLLISIONLESS DETRAPPING AND ENTRAPPING

In stellarators with the depth of the helical wells dependent on the minor radius, ions can collisionlessly detrap or entrap from the helical well as shown in Fig. 5. This can be understood as follows. Superposition of the grad-B drift upon the poloidal $\vec{E}_r \times \vec{B}$ drift results in an outward shift of the center of the trapped-ion drift orbit. Consequently, the depth of the helical well changes with the poloidal location of a trapped ion. Hence, barely trapped ions can experience collisionless detrapping and entrapping.

If the helical well depth $\epsilon_h(r) = \delta_a(r/a)^{\ell}$ with δ_a a constant,[4] then helically trapped ions with pitch angle $\xi = \sqrt{2\delta_a}(r_c/a)^{\ell/2}$ can detrap at radius r_c. The change in helical well depth $\delta\epsilon_h(r)$ and the corresponding collisionless change in the trapping condition $\delta\xi_{CL}$ as r changes by an amount δr is

$$\frac{\delta\epsilon_h(r)}{h(r)} = \frac{2\delta\xi_{CL}}{\xi}$$

$$= \ell\frac{\delta r}{r} \quad . \tag{A1}$$

Since the shift of the center of the trapped ion drift orbit from the center of the magnetic surface is v_E/Ω_E, the fraction of ions, F, that can experience collisionless detrapping and entrapping is $\underline{O}[(\ell/2)\sqrt{2\delta_a}(v_B/a\Omega_E)]$.

Collisions also bring ions in and out of helical wells. In one poloidal rotation period, collisions change the pitch angle of the ions by an amount

$$\delta\xi_{coll} = \underline{O}\left(\frac{\nu_i}{\Omega_E}\right)^{1/2} \quad . \tag{A2}$$

Therefore, in order for the effect of collisionless detrapping and entrapping to play a significant role in ion transport, the collisionless change in the trapped condition $\delta\xi_{CL}$ due to the radial variation of the depth of the helical well should be greater than $\delta\xi_{coll}$, i.e.,

$$\delta\xi_{coll} < \delta\xi_{CL}$$

$$= \frac{\ell}{2}\frac{\nu_B}{a\Omega_E}\left[2\delta_a\left(\frac{r}{a}\right)^{\ell}\right]^{1/2} \quad . \tag{A3}$$

If $\delta_a = 0.3$, then for the reference stellarator, the condition for Eq. (A3) to hold is that ion energy $\varepsilon > 3T$, and for the stellarator reactor, the condition is that $\varepsilon > 4T$. The parameters for the reference stellarator and the stellarator reactor are given in Table I.

To estimate the diffusion coefficient, we need to evaluate the step size δr. Using Eqs. (A1) and (A2), it can be shown that

$$\frac{\delta r}{r} \approx \frac{2}{\ell\xi_c}\left(\frac{\nu_i}{\Omega_E}\right)^{1/2},$$

and hence,

$$\delta r \approx \frac{2a}{\ell\sqrt{2\delta}}\left(\frac{\nu_i}{\Omega_E}\right) . \tag{A4}$$

The characteristic frequency $\overline{\nu}$ for a trapped ion to detrap is $\underline{0}(\Omega_E)$. Therefore, the diffusion coefficient is

$$D = \underline{0}(\delta r^2\overline{\nu F})$$

$$= \frac{V_B}{\Omega_E} \frac{a}{\sqrt{2\delta_a}} \nu_i \quad , \tag{A5}$$

for $\ell = 2$.

Note that the ion does not entrap in the lower region of the torus after collisionless detrapping from point A (see Fig. 12), because the rate of change in particle pitch angle due to collisions is slower than the rate of increase of the helical well strength as the particle drifts from an inner minor radius to an outer minor radius. Also note that even if the helical wells have poloidal symmetry, the probability for an ion to entrap at the poloidal location with poloidal angle θ, after detrapping at $-\theta$, is small due to pitch-angle scattering.

Kinetic calculations for the problem discussed in this appendix have been carried out be Mynick.[5] However, in Mynick's calculation, it is assumed that particles always entrap at θ after detrapping at $-\theta$. A correct treatment of this problem with pitch-angle scattering would be a good subject for investigation.

Even if ε_h is constant across the minor radius, it might still be thought that the magnetic field variation on the trapped ion drift orbit caused by the variation in the toroidal field strength would collisionlessly detrap and entrap ions. This is not generally the case because, if the helical well length is assumed to be independent of its poloidal location, then the effect is compensated by E_r. This can be seen from the following argument. As a trapped ion changes its radius by Δ, it changes its kinetic energy by an amount

$$\frac{m\delta v^2}{2} = e\Delta E_r \quad ,$$

$$= \frac{ev_B Br}{c} ,$$

$$= - \frac{mv_\perp^2}{2} \frac{r}{R_0} ,$$

in order to conserve total energy. But by the conservation of the first adiabatic invariant,

$$\delta\left(\frac{mv_\perp^2}{2}\right) = \frac{mv_\perp^2}{2} \frac{\delta B}{B} ,$$

$$= - \frac{mv_\perp^2}{2} \frac{r}{R_0} .$$

Thus, $v_\parallel^2$ is unchanged at corresponding points in the helical well. (This also follows from the conservation law for the second adiabatic invariant.) Now, for ϵ_h *independent of* r [*as in helical-axis stellarators* (Heliac)], the helical trapped-region in velocity space expands by an amount r/R_0 as one moves from the inner (smaller R) to the outer (larger R) region of the torus. At the same time, the ion perpendicular velocity is reduced by the same factor of r/R_0 as indicated above. As a result, the fraction of trapped ions remains constant and the toroidal magnetic field variation causes no detrapping or entrapping.

REFERENCES

1. D. D.-M. Ho and R. M. Kulsrud, Princeton Plasma Physics Laboratory Report No. PPPL-2253; to Phys. Fluids (to be published).
2. A. A. Galeev, R. Z. Sagdeev, H. P. Furth, and M. N. Rosenbluth, Phys. Rev. Lett. 22, 511 (1969).
3. A. A. Galeev and R. Z. Sagdeev, Review of Plasma Physics, edited by M. A. Leontovich (Consultants Bureau, New York, 1979), Vol. 7, p. 307.
4. A. I. Morozov and L. S. Solovev, Review of Plasma Physics, edited by M. A. Leontovich (Consultants Bureau, New York, 1966), Vol. 2, p. 1.
5. H. E. Mynick, Phys. Fluids 26, 2609 (1983).

TABLE I. STELLARATOR PARAMETERS

Physical quantity	Reactor	Reference stellarator	ATF[a]	Small[b] Heliac
Peak plasma density (cm^{-3})	6×10^{14}	2×10^{14}	10^{14}	10^{14}
Peak plasma temperature (keV)	10	10	1	1
Toroidal magnetic field (kG)	60	50	18	10
Peak β	13.4	6.4	2.5	8
R(m)	10	10	2.1	1.2
a(m)	1.0	1.0	0.3	0.25
h(r=a/2)	0.1	0.1	0.2	0.1
Deuteron thermal velocity ($cm \cdot sec^{-1}$)	1.1×10^{8}	1.1×10^{8}	3.4×10^{7}	3.4×10^{7}
Deuteron 90° deflection time (sec)	2.3×10^{-3}	7.0×10^{-3}	0.44×10^{-3}	0.44×10^{-3}

[a] Reference 12.
[b] Reference 18.

FIGURE CAPTIONS

Fig. 1 Toroidal coordinate system (r, θ, ζ).

Fig. 2 Projection of a typical collisionless ion orbit on a poloidal cross section. Point O is the center of the magnetic surface and $\Delta \equiv v_B/\Omega_E$.

Fig. 3 A and B as a function of pitch-angle parameter κ for ion energy at $\varepsilon = 4T$.

Fig. 4 (a). The relative ion particle flux per unit energy, $[x^{7/4}e^{-x}(\Phi(\sqrt{x}) - G(\sqrt{x}))^{1/2}(x - 3/2)]$, as a function of the normalized energy $x = \varepsilon/T$.

(b). The relative ion particle flux per unit energy, $[x^{11/4}e^{-x}(\Phi(\sqrt{x}) - G(\sqrt{x}))^{1/2}(x - 3/2)$, as a function of x.

Fig. 5 Projection of a typical collisionless ion orbit on a poloidal cross section with the effect of collisionless detrapping and entrapping. Point A is the collisionless entrapping point where toroidally trapped ions enter the helical well. Point B is the collisionless detrapping point where ions leave the helical well and become toroidally trapped particles. Point O is the center of the magnetic surface and $\Delta \equiv v_B/\Omega_E$.

#85T0118

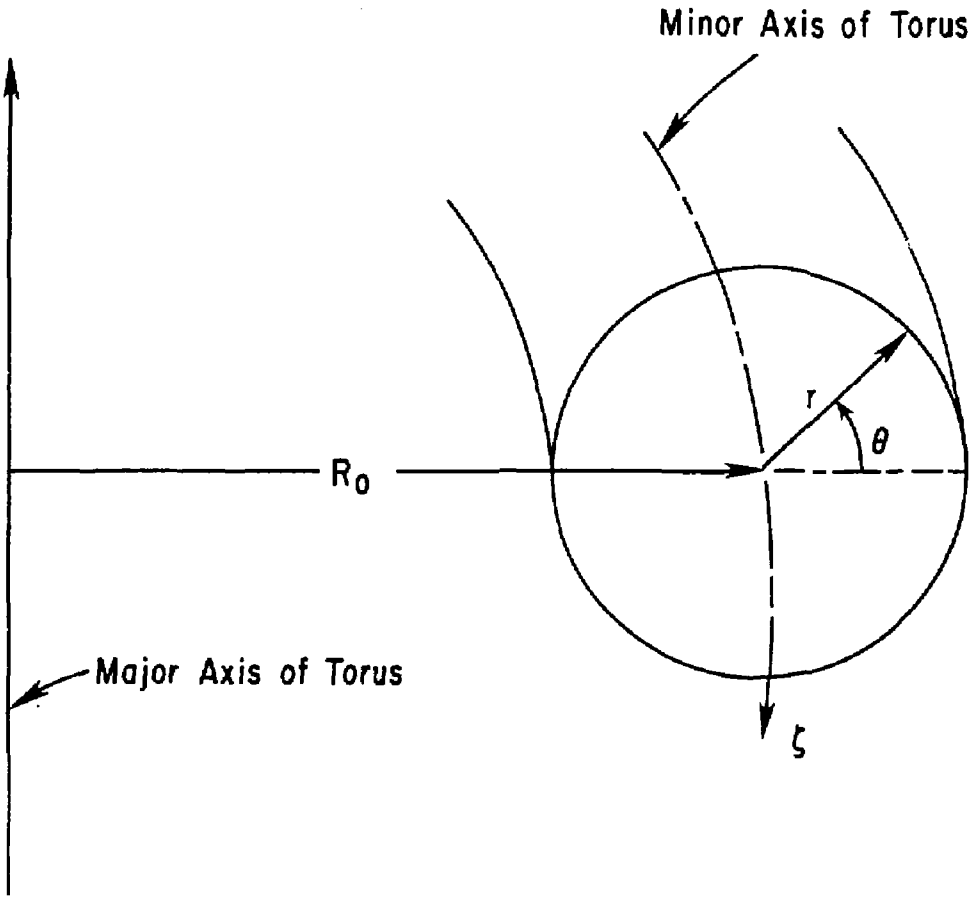

Fig. 1

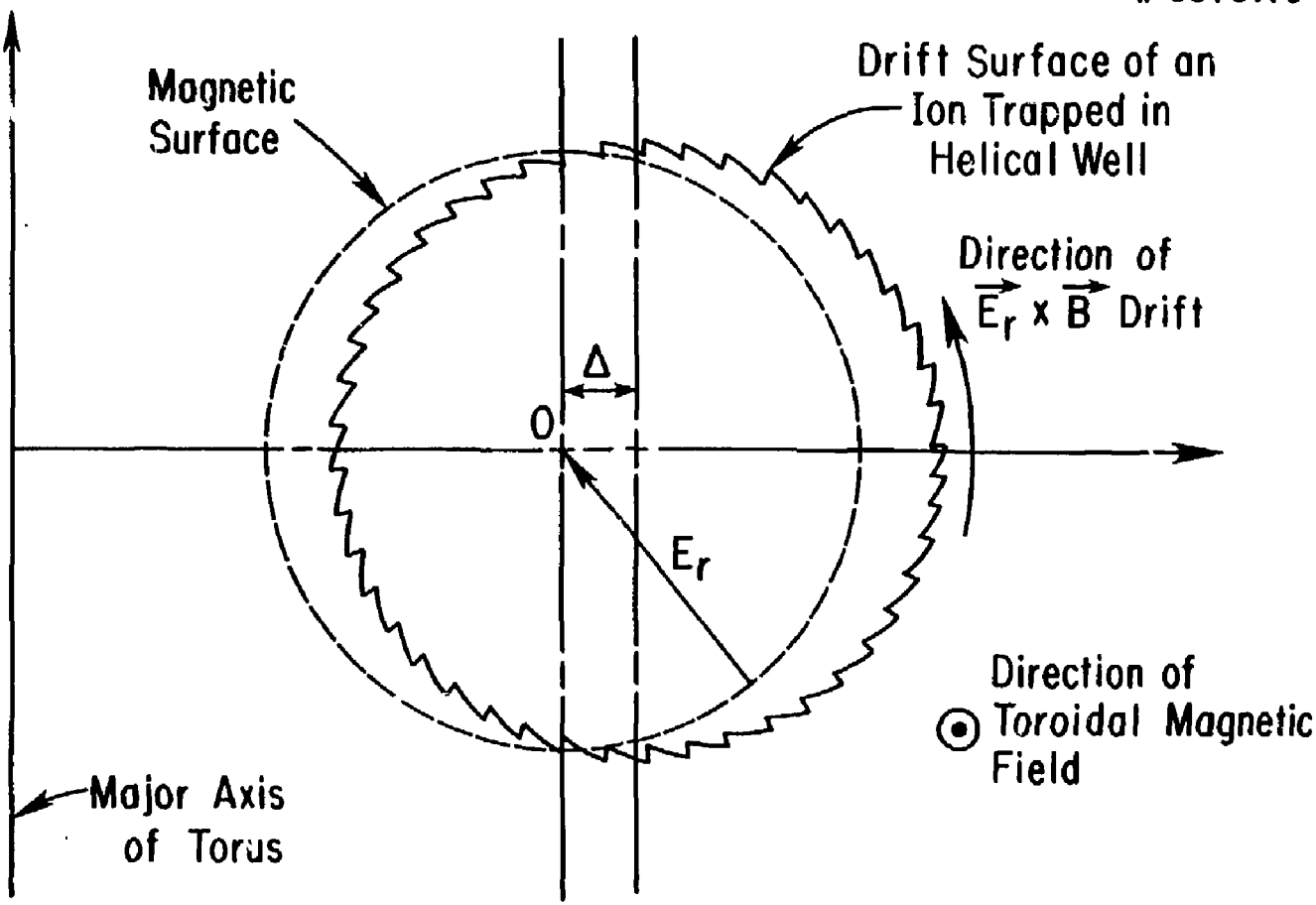
Magnetic Surface
Drift Surface of an Ion Trapped in Helical Well
Direction of $\vec{E}_r \times \vec{B}$ Drift
Δ
0
E_r
Direction of Toroidal Magnetic Field
Major Axis of Torus

Fig. 2

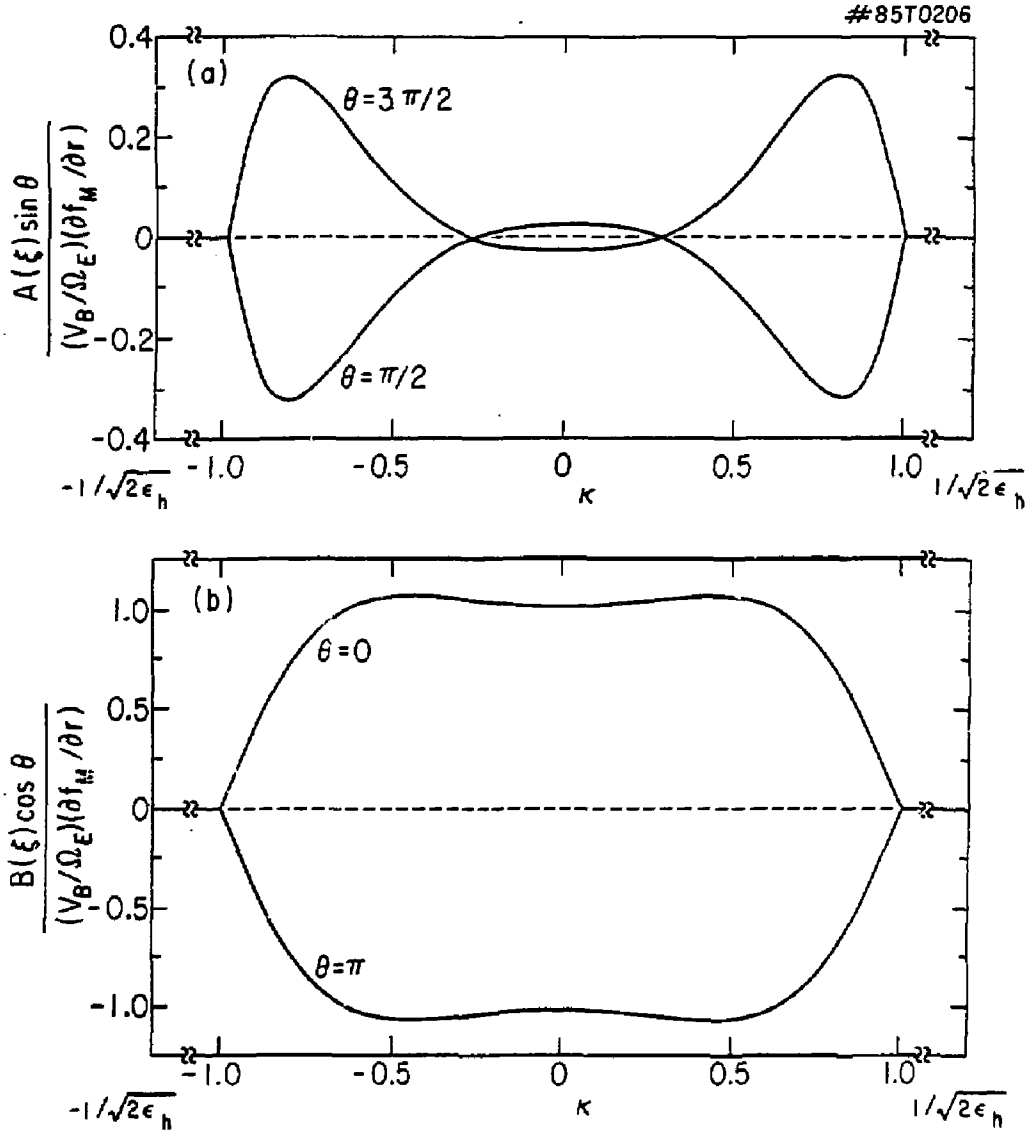
#85T0206
(a)
θ=3π/2
θ=π/2
A(ξ) sin θ / (V_B/Ω_E)(∂f_M/∂r)
0.4
0.2
0
-0.2
-0.4
-1.0
-0.5
0
0.5
1.0
κ
-1/√2ε_h
1/√2ε_h
(b)
θ=0
θ=π
B(ξ) cos θ / (V_B/Ω_E)(∂f_M/∂r)
1.0
0.5
0
-0.5
-1.0
-1.0
-0.5
0
0.5
1.0
κ
-1/√2ε_h
1/√2ε_h

Fig. 3

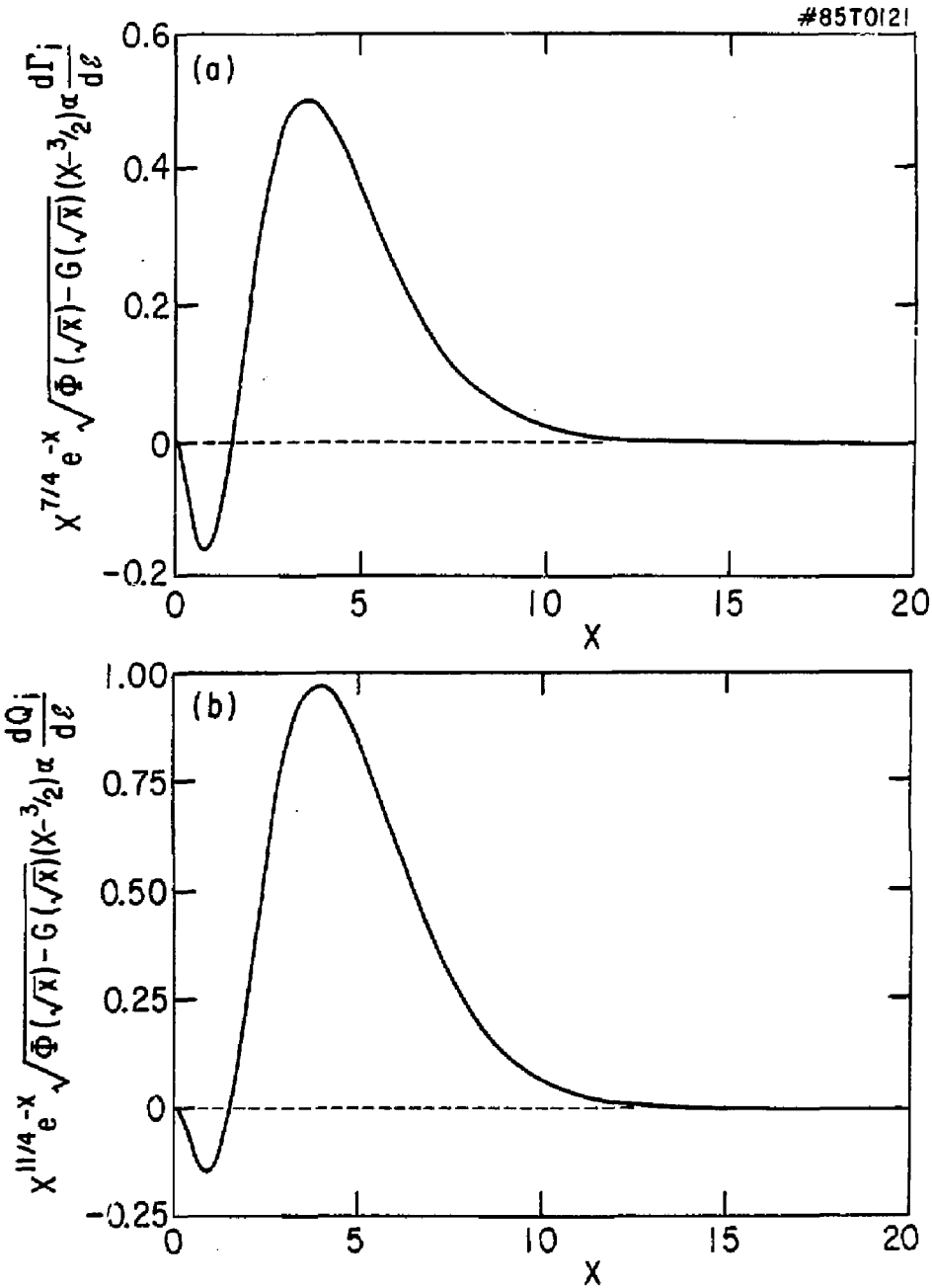
#85T0121
(a)
$X^{7/4}\, e^{-X} \sqrt{\Phi(\sqrt{X}) - G(\sqrt{X})}\,(X^{-3/2})^{\alpha} \frac{d\Gamma_i}{d\mathcal{E}}$
0.6
0.4
0.2
0
-0.2
0
5
10
15
20
X
(b)
$X^{11/4}\, e^{-X} \sqrt{\Phi(\sqrt{X}) - G(\sqrt{X})}\,(X^{-3/2})^{\alpha} \frac{dQ_i}{d\mathcal{E}}$
1.00
0.75
0.50
0.25
0
-0.25
0
5
10
15
20
X

Fig. 4

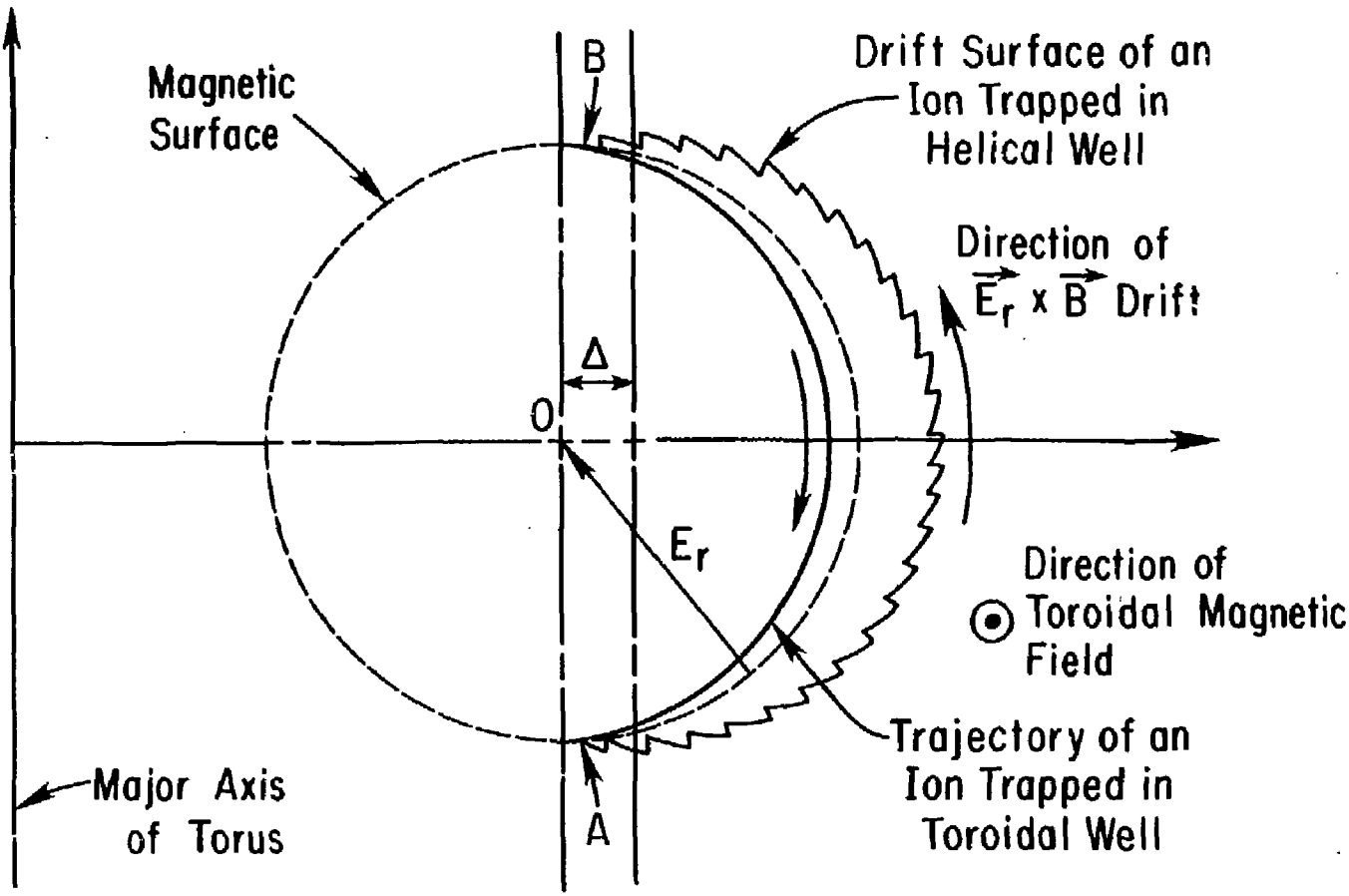
#85T0177
Magnetic Surface
B
Drift Surface of an Ion Trapped in Helical Well
Direction of $\vec{E}_r \times \vec{B}$ Drift
Δ
0
E_r
Direction of Toroidal Magnetic Field
Trajectory of an Ion Trapped in Toroidal Well
Major Axis of Torus
A

Fig. 5

EXTERNAL DISTRIBUTION IN ADDITION TO UC-20

Plasma Res Lab, Austra Nat'l Univ, AUSTRALIA
Dr. Frank J. Paoloni, Univ of Wollongong, AUSTRALIA
Prof. I.R. Jones, Flinders Univ., AUSTRALIA
Prof. M.H. Brennan, Univ Sydney, AUSTRALIA
Prof. F. Cap, Inst Theo Phys, AUSTRIA
Prof. Frank Verheest, Inst theoretische, BELGIUM
Dr. D. Palumbo, Dg XII Fusion Prog, BELGIUM
Ecole Royale Militaire, Lab de Phys Plasmas, BELGIUM
Dr. P.H. Sakanaka, Univ Estadual, BRAZIL
Dr. C.R. James, Univ of Alberta, CANADA
Prof. J. Teichmann, Univ of Montreal, CANADA
Dr. H.M. Skarsgard, Univ of Saskatchewan, CANADA
Prof. S.R. Sreenivasan, University of Calgary, CANADA
Prof. Tudor W. Johnston, INRS-Energie, CANADA
Dr. Hannes Barnard, Univ British Columbia, CANADA
Dr. M.P. Bachynski, MPB Technologies, Inc., CANADA
Chalk River, Nucl Lab, CANADA
Zhengzu Li, SW Inst Physics, CHINA
Library, Tsing Hua University, CHINA
Librarian, Institute of Physics, CHINA
Inst Plasma Phys, Academia Sinica, CHINA
Dr. Peter Lukac, Komenskeho Univ, CZECHOSLOVAKIA
The Librarian, Culham Laboratory, ENGLAND
Prof. Schatzman, Observatoire de Nice, FRANCE
J. Radet, CEN-BP6, FRANCE
AM Dupas Library, AM Dupas Library, FRANCE
Dr. Tom Mual, Academy Bibliographic, HONG KONG
Preprint Library, Cent Res Inst Phys, HUNGARY
Dr. S.K. Trehan, Panjab University, INDIA
Dr. Indra Mohan Lal Das, Banaras Hindu Univ, INDIA
Dr. L.K. Chavda, South Gujarat Univ, INDIA
Dr. R.K. Chhajlani, Vikram Univ, INDIA
Dr. B. Dasgupta, Saha Inst, INDIA
Dr. P. Kaw, Physical Research Lab, INDIA
Dr. Phillip Rosenau, Israel Inst Tech, ISRAEL
Prof. S. Cuperman, Tel Aviv University, ISRAEL
Prof. G. Rostagni, Univ Di Padova, ITALY
Librarian, Int'l Ctr Theo Phys, ITALY
Miss Clelia De Palo, Assoc EURATOM-ENEA, ITALY
Biblioteca, del CNR EURATOM, ITALY
Dr. H. Yamato, Toshiba Res & Dev, JAPAN
Direc. Dept. Lg. Tokamak Dev. JAERI, JAPAN
Prof. Nobuyuki Inoue, University of Tokyo, JAPAN
Research Info Center, Nagoya University, JAPAN
Prof. Kyoji Nishikawa, Univ of Hiroshima, JAPAN
Prof. Sigeru Mori, JAERI, JAPAN
Library, Kyoto University, JAPAN
Prof. Ichiro Kawakami, Nihon Univ, JAPAN
Prof. Satoshi Itoh, Kyushu University, JAPAN
Dr. D.I. Choi, Adv. Inst Sci & Tech, KOREA
Tech Info Division, KAERI, KOREA
Bibliotheek, Fom-Inst Voor Plasma, NETHERLANDS
Prof. B.S. Liley, University of Waikato, NEW ZEALAND
Prof. J.A.C. Cabral, Inst Superior Tecn, PORTUGAL
Dr. Octavian Petrus, ALI CUZA University, ROMANIA
Prof. M.A. Hellberg, University of Natal, SO AFRICA
Dr. Johan de Villiers, Plasma Physics, Nucor, SO AFRICA
Fusion Div. Library, JEN, SPAIN
Prof. Hans Wilhelmson, Chalmers Univ Tech, SWEDEN
Dr. Lennart Stenflo, University of UMEA, SWEDEN
Library, Royal Inst Tech, SWEDEN
Centre de Recherchesen, Ecole Polytech Fed, SWITZERLAND
Dr. V.T. Tolok, Kharkov Phys Tech Ins, USSR
Dr. D.D. Ryutov, Siberian Acad Sci, USSR
Dr. G.A. Eliseev, Kurchatov Institute, USSR
Dr. V.A. Glukhikh, Inst Electro-Physical, USSR
Institute Gen. Physics, USSR
Prof. T.J.M. Boyd, Univ College N Wales, WALES
Dr. K. Schindler, Ruhr Universitat, W. GERMANY
Nuclear Res Estab, Julich Ltd, W. GERMANY
Librarian, Max-Planck Institut, W. GERMANY
Bibliothek, Inst Plasmaforschung, W. GERMANY
Prof. R.K. Janev, Inst Phys, YUGOSLAVIA